ISSN 1674-1056
http://cpb.iphy.ac.cn
http://iopscience.iop.org/cpb
中国物理 B
Chinese Physics
中国物理
Chinese Physics B

Microdroplet targeting induced by substrate curvature

Hongguang Zhang(张红光), Zhenjiang Guo(郭振江), Shan Chen(陈珊), Bo Zhang(张博), Xianren Zhang(张现仁)

Citation: Chin. Phys. B . 2018, 27(9): 096801. **doi:** 10.1088/1674-1056/27/9/096801

Journal homepage: http://cpb.iphy.ac.cn; http://iopscience.iop.org/cpb

What follows is a list of articles you may be interested in

The properties of surface nanobubbles formed on different substrates

Zheng-Lei Zou(邹正磊), Nan-Nan Quan(权楠楠), Xing-Ya Wang(王兴亚), Shuo Wang(王硕), Li-Min Zhou(周利民), Jun Hu(胡钧), Li-Juan Zhang(张立娟), Ya-Ming Dong(董亚明)

Chin. Phys. B . 2018, 27(8): 086803. **doi:** 10.1088/1674-1056/27/8/086803

Mechanism of contact angle saturation and an energy-based model for electrowetting

Rui Zhao(赵瑞), Zhong-Cheng Liang(梁忠诚)

Chin. Phys. B . 2016, 25(6): 066801. **doi:** 10.1088/1674-1056/25/6/066801

Contact angle hysteresis in electrowetting on dielectric

Zhao Rui, Liu Qi-Chao, Wang Ping, Liang Zhong-Cheng

Chin. Phys. B . 2015, 24(8): 086801. **doi:** 10.1088/1674-1056/24/8/086801

Superamphiphobic, light-trapping $FeSe_2$ particles with a micro-nano hierarchical structure obtained by an improved solvothermal method

Yu Jing, Wang Hui-Jie, Shao Wei-Jia, Xu Xiao-Liang

Chin. Phys. B . 2014, 23(1): 016803. **doi:** 10.1088/1674-1056/23/1/016803

Fabrication of pillar-array superhydrophobic silicon surface and thermodynamic analysis on the wetting state transition

Liu Si-Si, Zhang Chao-Hui, Zhang Han-Bing, Zhou Jie, He Jian-Guo, Yin Heng-Yang

Chin. Phys. B . 2013, 22(10): 106801. **doi:** 10.1088/1674-1056/22/10/106801

Microdroplet targeting induced by substrate curvature*

Hongguang Zhang(张红光), Zhenjiang Guo(郭振江), Shan Chen(陈珊),
Bo Zhang(张博), and Xianren Zhang (张现仁)†

State Key Laboratory of Organic-Inorganic Composites, Beijing University of Chemical Technology, Beijing 100029, *China*

(Received 26 February 2018; revised manuscript received 7 May 2018; published online 10 August 2018)

Fundamental understanding of the wettability of curved substrates is crucial for the applications of microdroplets in colloidal science, microfluidics, and heat exchanger technologies. Here we report via lattice Boltzmann simulations and energetic analysis that microdroplets show an ability of transporting selectively to appropriate substrates solely according to substrate shape (curvature), which is called the substrate-curvature-dependent droplet targeting because of its similarity to protein targeting by which proteins are transported to the appropriate destinations in the cell. Two dynamic pathways of droplet targeting are identified: one is the Ostwald ripening-like liquid transport between separated droplets via evaporating droplets on more curved convex (or less curved concave) surfaces and growing droplets on less curved convex (or more curved concave) surfaces, and the other is the directional motion of a droplet through contacting simultaneously substrates of different curvatures. Then we demonstrate analytically that droplet targeting is a thermodynamically driven process. The driving force for directional motion of droplets is the surface-curvature-induced modulation of the work of adhesion, while the Ostwald ripening-like transport is ascribed to the substrate-curvature-induced change of droplet curvature radius. Our findings of droplet targeting are potentially useful for a tremendous range of applications, such as microfluidics, thermal control, and microfabrication.

Keywords: droplet targeting, substrate curvature, lattice Boltzmann simulation.

PACS: 68.08.Bc, 68.18.Jk, 82.65.+r **DOI:** 10.1088/1674-1056/27/9/096801

1. Introduction

The directional motion[1] of sessile droplets on solid surfaces has been an active topic for both experimental and theoretical investigations. In nature, surfaces that are capable of transporting liquid droplets are ubiquitous, such as butterfly wings,[2,3] rice leaves,[4,5] and feathers of ducks and geese.[6] Inspired by these surfaces, various methods have been developed to prepare surfaces with similar directional liquid transport ability,[7,8] which shows potential for a tremendous range of applications from anti-icing,[9,10] dip-pen nanolithography, to oil/water separation. On the one hand, solid surfaces with a specific curvature gradient are designed to collect the droplet through directional movement of droplets.[11–15] On the other hand, spontaneous motion of droplets has also been found on the heterogeneous substrates with wettability gradients.[16–21]

In this paper, we report via lattice Boltzmann simulations and energetic analysis that depending on their curvature, various substrates show different abilities for sorting droplets, i.e., droplets are capable of directional transportation targeting certain substrates with the appropriate shape (curvature). For the substrate-curvature-dependent droplet targeting, two dynamic pathways of droplet targeting are identified in this work: Ostwald ripening-like liquid transport between droplets without direct contact, and directional motion of droplets through contacting substrates of different curvatures simultaneously. Then we interpret the behaviors of droplet targeting as a result of free energy change due to the difference of substrate curvatures.

2. Model and simulation method

In the present work, the lattice Boltzmann (LB) method, a numerically robust technique[22,23] for simulating interfacial phenomena, was used to reveal the behaviors of the droplet targeting according to substrate curvature. We applied the three dimensional multicomponent and multiphase Shan–Chen (SC) type LB method[24,25] based on the D3Q19 lattice,[26] which has particularly been successfully used to study droplets wetting on spherical substrates.[27] In this model, a pseudopotential was employed to represent different interactions with the potential function of $V_{k\bar{k}}(x,x') = G_{k\bar{k}}(|x-x'|)\psi_k(x)\psi(x')$, where ψ_k represents the effective density of component k and the Green function $G_{kk'}$ determines the interaction strength between component k and $\bar{k}$ for neighboring lattice sites x and x'. For the version of the LB method used here, the density ratio and viscosity ratio for liquid and gas are both about 15. The details of the applied method can be found in our previous work.[28,29]

In this work, simulation boxes range from $100\times100\times70$ to $100\times100\times130$, in which one or two droplets interact selectively with substrates of different curvatures. All the quantities are reported here in dimensionless LB units. To simplify the description, we sometimes called the convex spherical sub-

*Project supported by the National Natural Science Foundation of China (Grant No. 91434204).
†Corresponding author. E-mail: zhangxr@mail.buct.edu.cn
© 2018 Chinese Physical Society and IOP Publishing Ltd

strates as colloids. Our extensive LB simulations reveal that microdroplets have the ability to select the substrates having an appropriate shape according to substrate curvature. The droplet selectivity of substrates is called droplet targeting or droplet sorting here, because of its similarity to protein targeting, by which proteins are transported to the appropriate destinations in the cell.

3. Results and analysis

3.1. Substrate-curvature-induced droplet targeting through the Ostwald ripening mechanism

Our simulations show that there exist at least two different pathways for droplet targeting. The first one resembles Ostwald ripening that refers to, e.g., in an emulsion system, the growth of large emulsions from those of smaller size because the larger emulsions are more energetically favorable than smaller ones. Different from emulsion coalescence for which neighboring emulsions come into direct contact and coalesce, Ostwald ripening occurs with the external environment (solvent) serving as the transfer medium. In our study, we also found similar behavior for sessile droplets without direct contact.

At the beginning of our simulations, for example, we placed two droplets of the same initial radius of $r_S = 15$ close to respectively the spherical colloid of a curvature radius $R = 30$ and a flat substrate (Fig. 1(a)). Note that the initial radius of a spherical droplet r_S, which was used here to represent the volume of sessile droplets, is different from the stable curvature radius for the same droplet when it sits on a substrate r. Since the material inherent hydrophobicities for the two substrates are the same, the only difference in Fig. 1(a) is the substrate curvature. Our simulation shows that although the two droplets are located far from each other, the droplets are transported through an Ostwald ripening-like manner so that the droplet on the flat substrate grows while the droplet on the convex colloid shrinks, indicating a net flux of liquid flowing between the two droplets without direct contact. As the simulation proceeded, the droplet on the convex colloid with a smaller curvature radius would finally disappear after a stage of continuous evaporation, and in contrast, the droplet on the flat substrate would keep stable after the growth stage (Fig. 1(a)).

The Ostwald ripening-like droplet targeting also occurs between two droplets placed respectively on a flat substrate and a concave spherical substrate (see Fig. 1(b)). Different from the droplet transport from more curved convex substrate to less curved ones (Fig. 1(a)), in this case the droplet on the flat substrate shrinks while the droplet on the concave substrate grows. This indicates that for concave substrates droplet stability increases as the curvature of concave substrates increases.

As a particular example, we simulated a vapor condensation process near a rough substrate having regions of different (convex, flat, and concave) local curvatures (see Fig. 1(c)). It is observed that initially the condensation took place both inside the concave part and near the corner where the convex part and the flat part join. However, as the simulation proceeded, the droplet on the flat region gradually disappeared and the droplet inside the cavity grew, confirming the droplet targeting via an Ostwald ripening-like mechanism (Fig. 1(c)). This observation also demonstrates that droplets show different stability depending on the local curvature of substrate on which the droplet sits.

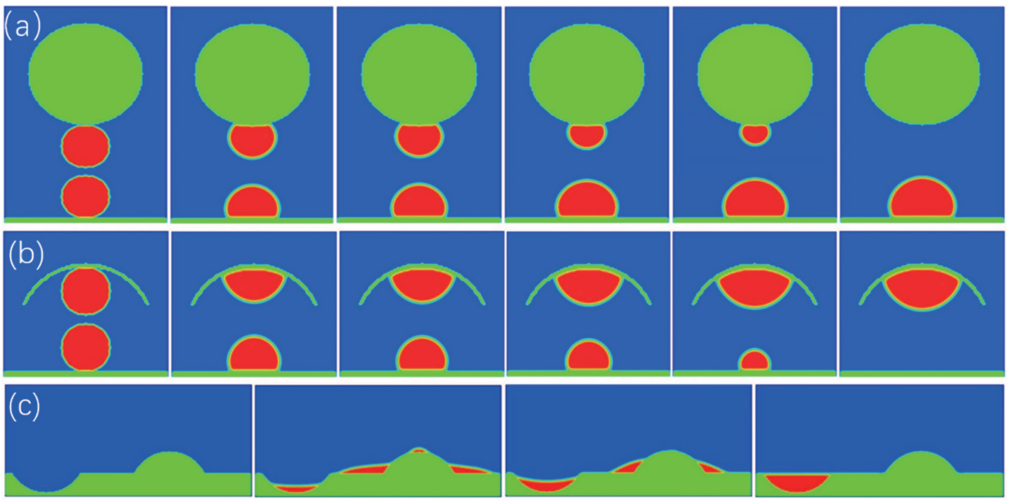


Fig. 1. (color online) Droplets on spherical substrates of different curvature radii showing curvature selectivity through Ostwald ripening-like transport. (a) The droplet of $r_S = 15$ on the flat substrate and the convex colloid ($R = 30$). The snapshots, from left to right, correspond to the time steps of 0, 6000, 14000, 19000, 21000, and 21800. (b) The droplet of $r_S = 15$ inside the spherical cavity (R =40) and on the flat substrate. The snapshots correspond to the time steps of 0, 900, 18000, 28000, 37000, and 40000. (c) During a condensation process, the transport between condensing droplets on a rough substrate having parts of different local curvature (the flat region and the convex and concave regions with a curvature radius of 40). The snapshots correspond to the time steps of 0, 2200, 7400, and 13800. In the figure, the solid surface has a wettability of $\theta_Y = 11\pi/18$.

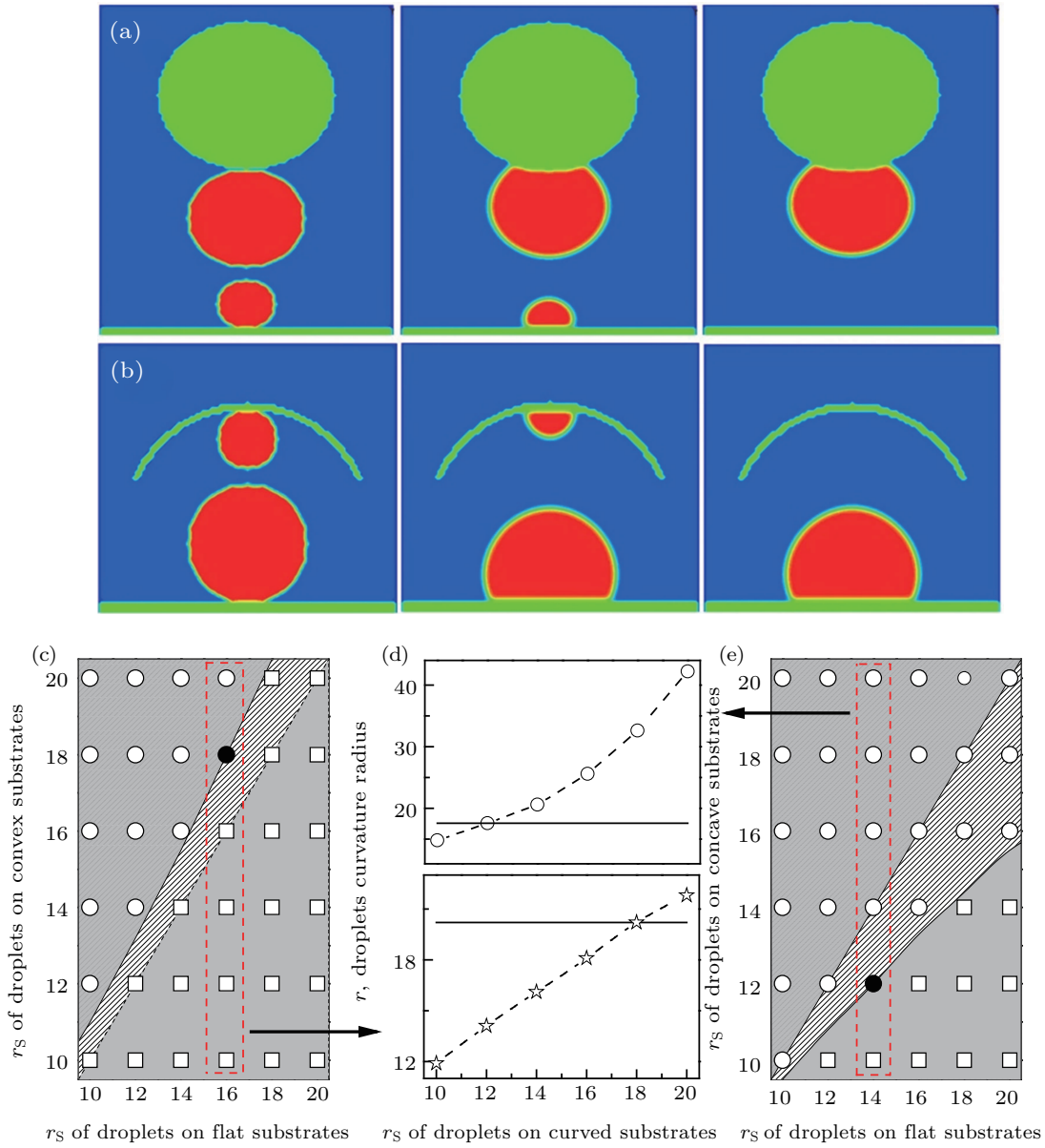


Fig. 2. (color online) (a) Liquid transport between the droplet of $r_S = 20$ on a convex colloid ($R = 30$) and the droplet of $r_S = 10$ on a flat substrate. The snapshots correspond to the time steps of 0, 2500, and 4000. (b) Liquid transport between the droplet of $r_S = 10$ inside a spherical cavity ($R = 40$) and the droplet of $r_S = 20$ on a flat substrate. The snapshots correspond to the time steps of 0, 3000, and 5000. In panels (a) and (b), the solid surfaces have a wettability of $\theta_Y = 11\pi/18$. Phase diagram for the direction of liquid transport via the Ostwald ripening-like pathway for two droplets on (c) a flat substrate and a convex substrate ($R = 30$) or (e) a flat substrate and a concave substrate ($R = 40$). The symbol □ denotes the corresponding simulation results for the liquid transferring toward the flat substrate, while the symbol ◯ for liquid transferring towards the curved substrate. To summarize the simulation results, the regions colored in light gray denote the simulated direction for liquid transferring from smaller droplets to larger droplets, while the shaded regions denote a reverse direction from larger droplets to smaller droplets. Note that the reverse transport towards the droplet of a smaller r_S does not mean the liquid transport towards the sessile droplet with a smaller curvature radius r. The symbol • shows the simulation results without apparent liquid transport during the simulation runs. (d) The radius of curvature for droplets on the curved substrates (measured before the transport begins), r, as a function of r_S, which was used to represent the droplet volume: (top) for droplets on concave substrates that are denoted in panel (e) and (bottom) for the droplets on convex substrates that are denoted in panel (c). As a comparison, solid lines in panel (d) show the curvature radii for the corresponding droplets on flat substrates. The solid substrates in panels (c)–(e) have a wettability of $\theta_Y = \pi/2$.

To reveal the mechanism of microdroplets targeting via a pathway of Ostwald ripening, we performed extensive simulations for different sized droplets on, respectively, a curved and a flat substrate (see, e.g., Figs. 2(a) and 2(b)). The summarized droplet transport directions are given in Figs. 2(c) and 2(e). The figures show that if their sizes differ significantly, liquid transport in a direction from the small droplets to the larger ones occurs. This clearly demonstrates the generality of droplet targeting. However, the figures also indicate that there exists a small regime of liquid transport showing a reverse direction from larger droplets to smaller droplets: a relatively larger droplet on the convex substrates transferring to the smaller droplet on flat substrates (Fig. 2(c)), or a relatively larger droplet on flat substrates transferring to the smaller droplet on concave substrates (Fig. 2(e)). Note that a similar phenomenon was found before for two-dimensional liq-

uid foams,[30] which was called the reverse Ostwald ripening that a large deformed bubble being adsorbed by the adjacent smaller bubble. We demonstrate here that although in the narrow regime (Figs. 2(c) and 2(e)) liquid transport can evolve beyond Ostwald ripening, or along a direction of reverse Ostwald ripening, the transport is indeed driven by droplet curvature. Figure 2(d), in which the initial curvature radii for droplets on curved substrates were measured before liquid transport began, demonstrates that the liquid transports are always along the direction towards the droplet with a larger radius of curvature, even in the regime with the reverse Ostwald ripening shown in Figs. 2(c) and 2(e). Therefore, the liquid is always transferred to the droplets with a larger curvature radius, but not necessarily the ones with a larger volume. As we will interpret below, the particular behavior of droplet targeting is ascribed to the substrate-curvature-induced change of droplet curvature, namely, the droplets of the same volume on substrates of different curvatures exhibit different curvature radii, causing the reverse Ostwald ripening-like transport.

We also investigated the dynamic characteristics of the processes, and the time evolution of free energy, contact angle, and curvature radius is shown in Figs. s1–s4 in the supporting information. As expected, during the processes of spontaneous transport, the free energy decreases with time, and the contact angle remains constant and is nearly equal to Young's contact angle θ_Y.

3.2. Substrate-curvature-induced droplet targeting through direct droplet movement

We also identified another pathway for droplet targeting the specific substrate according to substrate curvature: directional motion of a droplet that contacts simultaneously different substrates. For example, we initially placed a droplet with a radius $r_S = 15$ in between two spherical colloids having a radius of 10 and 30 (Fig. 3(a)). Again, the material inherent hydrophobicities for the two substrates were set to be the same (the same Young contact angle). For the initial configuration with an intermediate inter-colloid spacing, the droplet initially came into contact with both colloids, forming a liquid bridge. However, the two colloids having different curvatures exert different effects on the bridge, rendering a directional move of the liquid towards the colloid with a larger curvature radius ($R = 30$). As the simulation proceeded, the bridge changed its shape continuously, until the droplet completely left the smaller colloid and stuck to the larger one (Fig. 3(a)).

Similarly, when a droplet was initially placed into the confined space between a flat substrate and a spherical colloid with a curvature radius of $R = 30$, it would slowly leave the colloid and move to wet the flat substrate having an infinite large curvature radius (Fig. 3(b)). Again, the directional liquid transport is a result of the curvature difference between the two substrates, which changes the shape of the formed bridge continuously. Different from Fig. 3(a), the formed liquid bridge would rupture before the complete liquid transfer because the bridge reaches its mechanical instability, leaving a much smaller droplet on the convex substrate. The smaller droplet continued to transport to the larger one via Ostwald ripening. In comparison with $R = 10$ in Fig. 3(a), we ascribed the appearance of bridge rupture to the stronger adhesion from the less curved convex substrate ($R = 30$) in Fig. 3(b), which will be in detail discussed below. Then we simulated the movement of a droplet that initially contacted with both a flat substrate and a concave spherical substrate (Fig. 3(c)). The simulation results show that the droplet would finally leave the flat substrate and move to the concave substrate. All the simulation results demonstrate that the droplets can spontaneously transport to the substrate of appropriate curvature when it contacts simultaneously with two substrates having different curvatures.

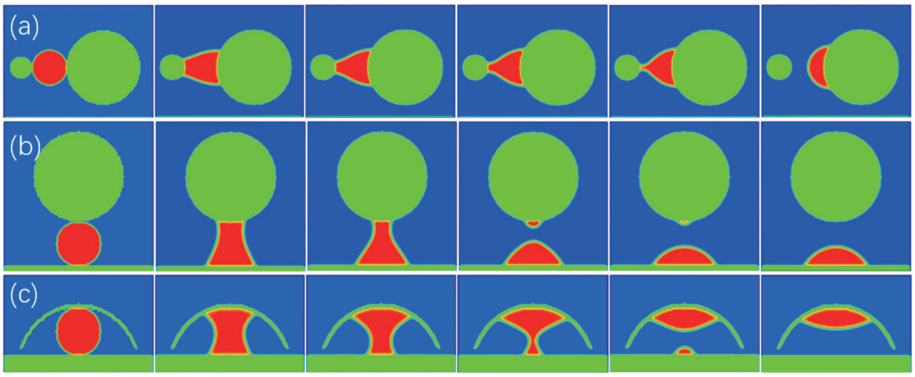


Fig. 3. (color online) Droplets on substrates of different radii showing curvature selectivity through direct liquid flow. (a) The movement of a droplet of $r_S = 15$ between two spherical colloids ($R = 10$ and $R = 30$). The snapshots, from left to right, correspond to the time steps of 0, 400, 800, 1200, 1500, and 2000. (b) The movement of a droplet between a flat substrate and a spherical colloid with a radius of $R = 30$. The snapshots correspond to the time steps of 0, 500, 1000, 1500, 1800, and 2400. (c) The movement of a droplet between a flat substrate and a spherical cavity with a radius of $R = 40$. The snapshots correspond to the time steps of 0, 200, 900, 1500, 1700, and 2200. In the figure, the solid surfaces have a wettability of $\theta_Y = \pi/3$.

3.3. Geometric relation and viability of Young's equation for droplets on spherical substrates

To interpret how the substrate geometry affects droplet targeting, we considered firstly whether Young's equation is affected by the curvature of spherical substrates. In fact, Wu *et al.*[31] have proved theoretically that Young's equation works for droplets on the convex and concave spherical surfaces, i.e., the contact angle of a sessile droplet on spherical surfaces satisfies $\cos\theta_{\rm Y} = \frac{\gamma_{\rm sv}-\gamma_{\rm sl}}{\gamma_{\rm lv}}$, with $\gamma_{\rm lv}$, $\gamma_{\rm sl}$, and $\gamma_{\rm sv}$ the interfacial tensions for the liquid–vapor, solid–liquid, and solid–vapor interfaces. For microdroplets we considered here that have a size of $\sim$ micrometers, the influences of gravity[28] and line tension can be safely ignored.[32] The viability of Young's equation makes it possible to analyze theoretically the driving force for droplet targeting.

To distinguish the driving force for the Ostwald ripening-like transport and the surface-curvature-induced droplet movement observed in our simulations, we need to determine theoretically the geometric features of different sessile droplets on substrates with various curvatures as well as the corresponding free energy. As usual, we assumed that the sessile droplets considered have a constant volume and their vapor–liquid interfaces are of spherical shape. The volume V for a droplet having an apparent contact angle θ and a curvature radius r is given by

$$\begin{aligned} V &= \frac{1}{3}\pi r^3[2+3\cos\beta-(\cos\beta)^3] \\ &\quad -\frac{1}{3}\pi R^3[2-3\cos\alpha+(\cos(\alpha)^3], \end{aligned} \tag{1}$$

where R is colloid radius and $\theta^0 = \theta+\alpha$ with α the cone angle for the colloid surface covered by the droplet (see Fig. 4). From the geometric relationships shown in Fig. 4, we have $\cos\alpha = \frac{(R^2+c^2-r^2)}{2Rc}$, $R\sin\alpha = r\sin\beta$, and $\cos\beta = \frac{(r^2+c^2-R^2)}{2rc}$ with $c = \sqrt{r^2+R^2-2rR\cos\theta}$ and $\beta+\theta^0 = \pi$. By substituting the geometric relationships into Eq. (1), the droplet volume can be determined as a function of r and θ.

For a droplet placed on a spherical surface, the total free energy G reads

$$G = \gamma_{\rm lv}A_{\rm lv} + (\gamma_{\rm sl}-\gamma_{\rm sv})A_{\rm sl}. \tag{2}$$

Note that the equation is valid for finite surfaces. In the equation, $A_{\rm lv}$ and $A_{\rm sl}$ denote the areas for liquid–vapor and solid–liquid interfaces, which can be determined as $A_{\rm lv} = 2\pi r^2(1-\cos\theta^0)$ and $A_{\rm sl} = 2\pi R^2[1-\cos(\theta^0-\theta)]$. In fact, $\mathrm{d}G(r,\theta) = 0$ under the constraint of $\mathrm{d}V(r,\theta) = 0$ can give the Young equation, as demonstrated by Wu *et al.*[31] Therefore, in the case of ignoring line tension, the curvature of spherical substrates does not change the contact angle of sessile droplets, $\theta = \theta_{\rm Y}$.[31] Similarly, for a spherical concave substrate (spherical cavity as shown in Fig. 4(b)), it can be proved in a similar way that Young's equation holds again.

For a droplet with a given volume V, we can determine the unknown variables α and r according to Eq. (1) because of $\theta = \theta_{\rm Y}$. Hence, the total free energy G for the droplet on a spherical colloid can be determined with

$$\begin{aligned} G &= \gamma_{\rm lv}(A_{\rm lv}-\cos\theta A_{\rm sl}) \\ &= 2\pi\gamma_{\rm lv}[r^2(1-\cos\alpha\cos\theta+\sin\alpha\sin\theta) \\ &\quad -\cos\theta R^2(1-\cos\alpha)]. \end{aligned} \tag{3}$$

We also considered another situation of curved substrates: spherical cavity. Similarly, the total free energy for the droplet with the given volume that sits inside the cavity can be determined because of the known contact angle $\theta = \theta_{\rm Y}$.

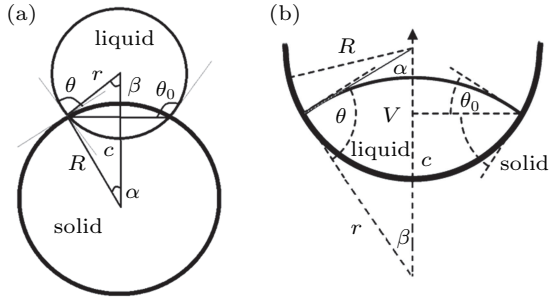


Fig. 4. Schematic illustration of the wetting of a liquid droplet on (a) the outer surface of a spherical colloid and (b) the inner surface of a spherical cavity.

3.4. Theoretical analysis of the driving force for droplet targeting

To interpret the substrate-curvature-induced droplet targeting, we calculated the free energy of a droplet on various colloids of different curvatures. As a comparison, the free energy for a droplet sitting on a flat surface can be obtained[15] from $G_{\rm f} = \frac{3V\gamma_{\rm lv}}{r_{\rm f}}$, with $r_{\rm f}$ the radius of the droplet on a flat surface that has a relationship with the radius of the fully spherical droplet of the same volume, $r_{\rm S}$, according to

$$\frac{r_{\rm S}}{r_{\rm f}} = \left[\frac{(1-\cos\theta_{\rm Y})^2(2+\cos\theta_{\rm Y})}{4}\right]^{1/3}.$$

Figure 5(a) gives the reduced free energy $G/G_{\rm f}$ of sessile droplets as a function of the curvature radius of convex substrates on which droplets sit. The figure indicates that for the droplet of the same volume on colloids having the same wettability (the same $\theta_{\rm Y}$), the surface free energy G decreases with the increase of substrate curvature radius. This observation demonstrates that droplet stability is enhanced with the increase of the curvature radius of substrates, and therefore this finding can interpret the LB simulation results that droplets can spontaneously target convex surfaces having a larger curvature radius (Fig. 1(a), Figs. 2(a) and 2(c), and Figs. 3(a) and 3(b)). For concave substrates, figure 5(b) shows that the surface free energy G increases with the increase of substrate curvature radius, meaning the decrease of droplet stability as

the curvature radius of the concave substrates increases. This again agrees with LB observations (Fig. 1(b), Figs. 2(b) and 2(e), and Fig. 3(c)).

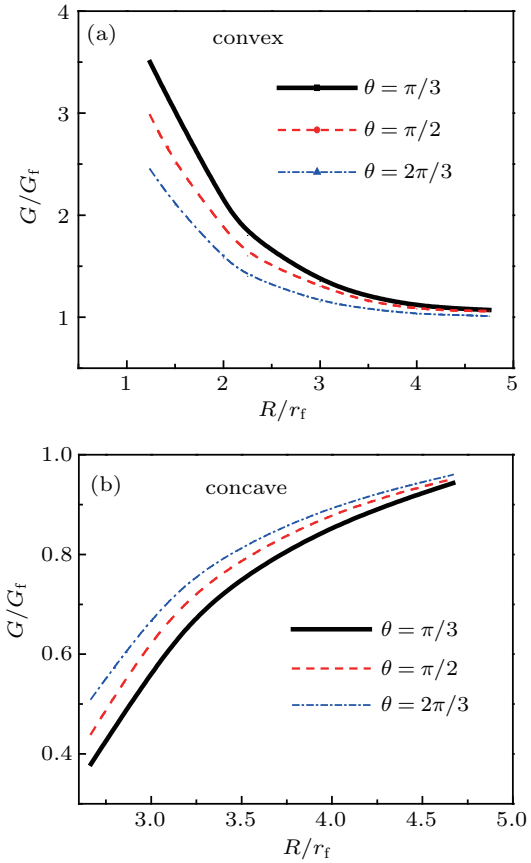


Fig. 5. (color online) The dimensionless G/G_f as a function of reduced colloid radius R/r_f of (a) spherical colloid and (b) spherical cavity. Here r_f and G_f are the curvature radius and free energy for the droplet with the same volume on the flat substrate.

Above we show that the droplet targeting is a thermodynamically-driven process. More specifically, here we ascribed the difference of the work of adhesion to the driving force for the surface-curvature-induced directional droplet motion (Fig. 3). We calculated the work of adhesion on different curved surfaces, given as

$$W = \gamma_{lv} A_{sl} (1 + \cos\theta). \tag{4}$$

On a convex spherical substrate, the work of adhesion of droplets is given by $W = \gamma_{lv} 2\pi R^2 (1 - \cos\alpha)(1 + \cos\theta)$. As a comparison, the corresponding work of adhesion on a flat substrate is determined as $W_f = \gamma_{lv} \pi r^2 \sin^2\theta (1 + \cos\theta)$. The change of adhesion work with substrate curvature radius is shown in Fig. 6(a), from which we can find that the work of adhesion increases with the curvature radius of convex substrates. Consequently, the liquid will migrate along the direction for increasing the work of adhesion. Consistently, the simulation results show that the liquid will gradually migrate to the convex substrate with a larger curvature radius (Figs. 3(a) and 3(b)). Similarly, for a droplet on concave substrates, the work of adhesion decreases as the increase of substrate curvature radius (Fig. 6(b)). This agrees with the simulation observation in Fig. 3(c). Therefore, the simulation results and the theoretical analysis agree well with each other.

For the driving force of the Ostwald ripening-like transport, we ascribed the increase of stability of the sessile droplets to the increase of droplet curvature radius on less curved convex (or more curved concave) substrates (Figs. 6(c) and 6(d)), which results in the decrease in Laplace pressure since $\Delta P \sim 1/r$. In detail, on a convex substrate, the droplet shows an increase in curvature radius as the substrate becomes less curved (Fig. 6(c)). Therefore, it is the difference of curvature radii between droplets that causes the droplet on the more curved convex substrate to dissolve and the one on the less curved substrate to grow (Figs. 1(a) and 2(c)). In contrast, on concave substrates, the curvature radius of a droplet increases as the substrate becomes more curved (Fig. 6(d)), which induces the growth of the droplet on the more curved substrate and the gradual disappearance of the droplet on a less curved substrate (Figs. 1(b) and 2(e)). Thus the same droplet on substrates of different curvatures exhibits different curvature radii, and therefore different effective pressures for vapor around the droplet. More interestingly, this sometimes causes the transport of liquid from a larger sessile droplet to a smaller sessile droplet, namely, the reverse Ostwald ripening as shown in the shaded regions of Figs. 2(c) and 2(e), because the curvature radius of the larger droplet may become relatively smaller than that for the smaller droplet when they sit respectively on substrates of different curvature (Fig. 2(d)).

The Ostwald ripening-like transport found here, including the reverse Ostwald ripening, originates from different curvature radii among droplets, or equivalently, the different pressures of vapor around the droplets of different curvatures since the Laplace pressure $\Delta P \sim 1/r$, which means that the pressure of the surrounding vapor in equilibrium with a droplet of larger curvature radius is lower than that for a droplet of smaller curvature radius. Therefore, the liquid is always transferred to the droplets with a larger curvature radius, but not necessarily the ones with a larger volume, because the droplets of the same volume on substrates of different curvatures could exhibit different curvature radii. This is why the reverse Ostwald ripening occurs. For droplets sitting respectively on substrates of different curvatures, in some cases the curvature radii of larger droplets may become relatively smaller than those for the smaller droplets, which leads to the reverse Ostwald ripening-like transport.

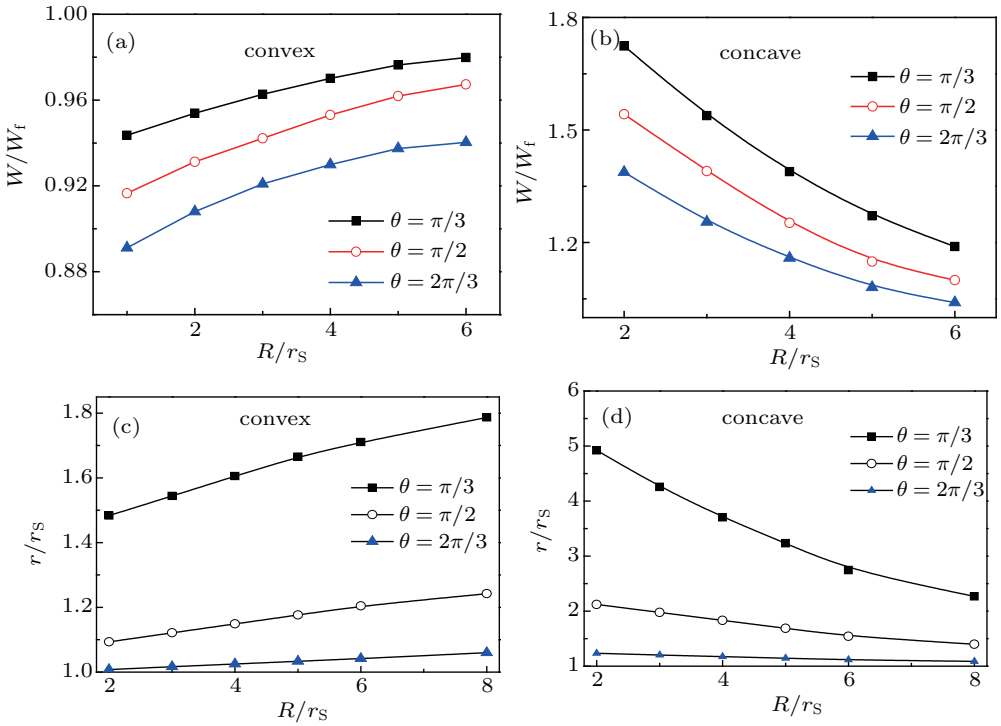


Fig. 6. (color online) (a), (b) The work of adhesion W and (c), (d) curvature radius r of droplets as a function of the radius of the convex and concave spherical substrates. Here, W_f is the adhesion work for a droplet of the same volume at the flat substrate, and r_S is the corresponding radius of a spherical droplet that has the same volume.

4. Conclusion

We report via lattice Boltzmann simulations that droplets show an ability of selectively targeting the substrate with appropriate curvature. Simulation results show that there exist at least two pathways for the behavior of droplet targeting: Ostwald ripening-like liquid transport between separated droplets and directional motion of droplets via simultaneously contacting substrates of different curvatures. Then we demonstrate through theoretical analysis that droplet targeting is a thermodynamically-driven process. The directional motion of droplets is ascribed to the difference of the work of adhesion for the droplet contacting with substrates of different curvature, while the Ostwald ripening-like transport is ascribed to the change of droplet curvature radius depending on substrate curvature.

References

[1] Li J, Hou Y, Liu Y, Hao C, Li M, Chaudhury M K, Yao S and Wang Z K 2016 *Nat. Phys.* **12** 606
[2] Zheng Y, Gao X and Jiang L 2007 *Soft Matter* **3** 178
[3] Liu M, Zheng Y, Zhai J and Jiang L 2010 *Acc. Chem. Res.* **43** 368
[4] Feng L, Li S, Li Y, Li H, Zhang L, Zhai J, Song Y, Liu B, Jiang L and Zhu D 2002 *Adv. Mater.* **14** 1857
[5] Sun T, Feng L, Gao X and Jiang L 2005 *Acc. Chem. Res.* **38** 644
[6] Kennedy R J 1970 *Nature* **227** 736
[7] Wu H, Zhang R, Sun Y, Lin D, Sun Z, Pan W and Downs P 2008 *Soft Matter* **4** 2429
[8] Malvadkar N A, Hancock M J, Sekeroglu K, Dressick W J and Demirel M C 2010 *Nat. Mater.* **9** 1023
[9] Zhang Q, He M, Chen J, Wang J, Song Y and Jiang L 2013 *Chem. Commun.* **49** 4516
[10] Chen Y, Liu G C, Jiang L, Kim J Y, Ye F, Lee J K, Wang L and Wang B 2017 *Chin. Phys. B* **26** 046801
[11] Lorenceau É and Quéré D J 2004 *Fluid Mech.* **29** 510
[12] Hanumanthu R and Stebe K J 2006 *Colloid. Surf. A* **282** 227
[13] Liu J L, Xia R, Li B W and Feng X Q 2007 *Chin. Phys. Lett.* **24** 3210
[14] Michielsen S, Zhang J, Du J and Lee H J 2011 *Langmuir* **27** 11867
[15] Lv C, Chen C, Chuang Y C, Tseng F G, Yin Y, Grey F and Zheng Q 2014 *Phys. Rev. Lett.* **113** 026101
[16] Scriven L E and Sternling C V 1960 *Nature* **187** 186
[17] Cazabat A M, Heslot F, Troian S M and Carles P 1990 *Nature* **346** 824
[18] Hancock M J, He J, Mano J F and Khademhosseini A 2011 *Small* **7** 892
[19] Malouin Jr B A, Koratkar N A, Hirsa A H and Wang Z 2010 *Appl. Phys. Lett.* **96** 234103
[20] Vaikuntanathan V, Kannan R and Sivakumar D 2010 *Colloid. Surf. A* **369** 65
[21] Wu J, Ma R, Wang Z and Yao S 2011 *Appl. Phys. Lett.* **98** 204104
[22] Zhang W, Wang Y and Qian Y H 2015 *Chin. Phys. B* **24** 064701
[23] Esfahanian V, Dehdashti E and Dehrouye-Semnani A M 2014 *Chin. Phys. B* **23** 084702
[24] Shan X and Chen H 1993 *Phys. Rev. E* **47** 1815
[25] Martys N S and Chen H 1996 *Phys. Rev. E* **53** 743
[26] Huang H, Thorne Jr D T, Schaap M G and Sukop M C 2007 *Phys. Rev. E* **76** 066701
[27] Hyväluoma J and Timonen J 2009 *J. Stat. Mech. -Theory E* **2009** P06010
[28] Zhang B, Lei Q, Wang Z and Zhang X 2015 *Langmuir* **32** 346
[29] Zhang B, Chen X, Dobnikar J, Wang Z and Zhang X 2016 *Phys. Rev. Fluids* **1** 073904
[30] Huang Z, Su M, Yang Q, Li Z, Chen S, Li Y, Zhou X, Li F and Song Y 2017 *Nat. Commun.* **8** 14110
[31] Wu D, Wang P, Wu P, Yang Q, Liu F, Han Y, Xu F and Wang L 2015 *Chem. Phys.* **457** 63
[32] Liu Y, Wang J and Zhang X 2013 *Sci. Rep.* **3** 2008